On the magnetization chaotic dynamics in the ferromagnetic resonance region

A.B. Borisov[a], B.N. Filippov[a], V.V. Zverev[b] and B.Y. Rubinstein[a]

[a] *Institute of Metal Physics, GSP-170, 620219 Ekaterinburg, Russia*
[b] *Department of Higher Mathematics, Ural Politechnical Institute, K-2, 620002 Ekaterinburg, Russia*

Journal of Magnetism and Magnetic Materials, **110**, pp.202-208 (1992)

Abstract

The regular and chaotic motion of the magnetization vector in the uniaxial ferromagnet is investigated. The various configurations of the external magnetic field applied to the magnet are considered. Numerical 'results are presented and different types of the dynamics are discussed.

1 Introduction

In recent years chaotic motion in deterministic nonlinear systems is getting continuous attention. It is evident today that chaotic behaviour is not an exceptional phenomenon and is widely spread in nature. Chaotic motion in the above-mentioned sense is discovered in biological, chemical, physical and other systems (see refs. [1]-[3]). Although chaotic behaviour is typical for highly nonlinear dynamical systems, usually it is impossible to obtain the corresponding analytical solutions of the dynamical equations, so that the most effective approach for investigations in this field is the numerical analysis of the simple nonlinear models. Now it is realized that low-dimensional models (with discrete or continuous time scale) are an important laboratory for nonlinear studies. In our opinion phenomenological models of magnetic media are appropriate for study of the chaotic dynamics. Various types of nonlinear behaviour as magnetic resonance, spin wave parametric generation, soliton motion, etc. have been studied intensively. However, as we know, routes to chaos and chaotic dynamics (including Feigenbaum period doubling, intermittency and so on) were not observed experimentally and investigated theoretically.

In this paper we shall study the magnetization dynamics in a ferromagnet using the Landau-Lifshitz equation [4] (LL model). We restrict our consideration to the spatially homogeneous case and so neglect the spin wave excitation process and other spatio-temporal phenomena. Of course, it may be incorrect in some real physical situations when the magnetization deviation from the initial equilibrium state is not small and the homogeneous rotation is unstable. However, we think that in any case it is important to study qualitative pecularities of dynamics for the simplest and fundamental physical models such as the homogeneous LL model of a ferromagnet. Moreover, we can hope that our approach also gives a proper description for some experimentally realized situations. For example, we can indicate at least one case when homogeneous rotation (without the magnetization breaking and the domain creation) was observed experimentally in a system being far from the equilibrium state; this is the impulse

remagnetization of the thin magnetic films (TMF) [5]-[10]. This phenomenon and also the local remagnetization of the film are interesting in view of practical applications of the TMF in the magneto-optical memory units (see ref. [11]). In the present paper we focus on the LL model for a ferromagnet with uniaxial anisotropy. Note that our results may be valid also for ferrimagnets and weak ferromagnets.

2 Equations of motion

We consider a spatially homogeneous evolution of the magnetization in a ferromagnet using the Landau-Lifshitz equation with the Hilbert dissipation term [12]:

$$d\mathbf{M}/dt = -\gamma[\mathbf{M} \times \mathbf{H}_{\text{eff}}] + \alpha M_s^{-1}[\mathbf{M} \times d\mathbf{M} \times /dt]. \tag{1}$$

In this equation γ is the gyromagnetic constant and a the relaxation parameter; $\mathbf{M} = \sum_{i=1}^{3} M_i \mathbf{e}_i$ is the magnetization vector ($|\mathbf{M}| = M_s$ is conserved); vectors $\mathbf{e}_i, i = 1, 2, 3$, compose the orthonormal basis in space. In the uniaxial anisotropy case $\mathbf{H}_{\text{eff}} = H(t) - \beta M_3 \mathbf{e}_3$ where $H(t) = H_0 + H_{\text{rf}}(t)$ is the external time dependent magnetic field and β is the anisotropy parameter (we consider an easy axis case $\beta < 0$). Eq. 1 can be rewritten in the form:

$$\frac{dm_i}{d\tau} = \frac{1}{1+\alpha^2} \left\{ q_i + \alpha \sum_{j,k=1}^{3} \epsilon_{ijk} m_j q_k \right\}, \quad i = 1, 2, 3 \tag{2}$$

where

$$q_i = \sum_{j,k=1}^{3} \epsilon_{ijk} (\delta_{j3} m_j m_k + m_j h_k),$$

ϵ_{ijk} is the unit antisymmetric tensor; δ_{ik} is the Kronecker delta symbol; $\mathbf{m} = \mathbf{M}/M_s, |\mathbf{m}| = 1, \mathbf{h}(t) = \mathbf{h}_0 + \mathbf{h}_{\text{rf}}(t) = \mathbf{H}/\beta M_s, \tau = \omega_0 t$ and $\omega_0 = \gamma \beta M_s$. In this paper we investigate the magnetization behaviour in the long-time asymptotics (*i.e.*, when the initial conditions are forgotten) supposing that the external magnetic field is of the order βM_s. We analyse several configurations in space:

(i) $\mathbf{h}_0 = \mathbf{e}_3 h_0$ lies along the anisotropy axis $\mathbf{e}_3$ and $\mathbf{h}_{\text{rf}} = \mathbf{e}_1 h_{\text{rf}} \cos \omega\tau$ lies in the orthogonal $(\mathbf{e}_1, \mathbf{e}_2)$ plane; here h_0 and h_{rf} are the time-independent amplitudes;

(ii) $\mathbf{h}_{\text{rf}} = \mathbf{e}_3 h_{\text{rf}} \cos \omega\tau$ lies along the anisotropy axis and $\mathbf{h}_0 = \mathbf{e}_1 h_0$ lies in the orthogonal $(\mathbf{e}_1, \mathbf{e}_2)$ plane;

(iii) the magnetization is driven by the pulsing magnetic field $\mathbf{h}_{\text{rf}} = \mathbf{e}_1 h_{pa}(\tau)$ having the rectangular pulse form; this field lies in the $(\mathbf{e}_1, \mathbf{e}_2)$ plane and has the amplitude h_{pa} where $h_{pa} \gg \beta M_s$, (anisotropy of light plane type).

The habitual conclusion getting from the linear FMR theory consists in the statement that both linearly oscillating and rotating magnetic fields cause almost identical resonant phenomena. Note that in our highly nonlinear case this statement is wrong. Taking into account the time dependence of the coefficient in (2) and the conservation law $|\mathbf{M}| = M_s$, we can deduce that in general the system under investigation has 3/2 degrees of freedom. However, if the driving field rotates in the $(\mathbf{e}_1, \mathbf{e}_2)$ plane: $h_1 + ih_2 = h_+ e^{i\omega\tau}$ (h_+ is constant), the equations of motion (2) takes the form

$$\begin{aligned} \frac{dm_+}{d\tau} - i\omega m_+ &= \frac{1}{1+\alpha^2} [i(1 + i\alpha m_3)((h_3 - m_3)m_+ - m_3 h_+) - \\ &\quad \alpha m_+ (m_+ h_- - m_- h_+)/2] \end{aligned} \tag{3a}$$

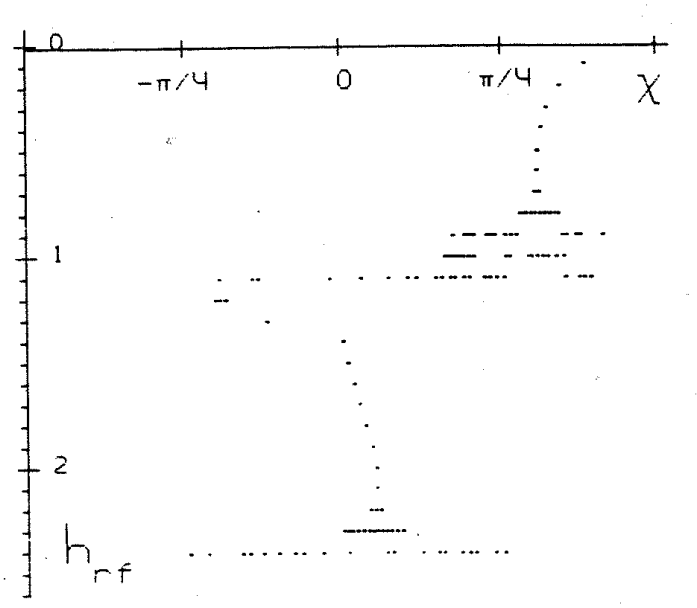

Figure 1: Bifurcation diagram for the case (i) for $h_0 = 0$. The points on the horizontal show $\chi(\tau_N)$ for $\tau_N = N\tau_{\rm rf}, N = 1, 2, 3, \ldots$ and for fixed $h_{\rm rf}$ values.

$$\frac{dm_+}{d\tau} = \frac{1}{2(1+\alpha^2)}\left[\alpha(h_3 - m_3)m_+m_- + im_-h_+(1+i\alpha m_3) + c.c.\right] \tag{3b}$$

in the rotating frame (here $m_+ = (m_1 + im_2)e^{-i\omega\tau}, m_- = (m_+)^*, h_- = (h_+)^*$). Coefficients in (3) are time-independent and so we deal now with the nonlinear system having only one degree of freedom. It is well-known that in this case the dynamical stochastization is impossible. In this paper we will investigate more closely a general situation.

For any case (i)-(iii) one can integrate the eqs. (2) using numerical procedures, but in the case (iii) it is more convenient to employ the analytical formulae. Let

$$\begin{aligned} m_1(\tau) &= \cos\chi(\tau)\cos\psi(\tau) = \sin\theta(\tau), \\ m_2(\tau) &= \cos\chi(\tau)\sin\psi(\tau) = \cos\theta(\tau)\sin\phi(\tau), \\ m_3(\tau) &= \sin\chi(\tau) = \cos\theta(\tau)\cos\phi(\tau). \end{aligned} \tag{4}$$

Using angular variables defined by (4) we can integrate the eqs. (2) straightforwardly. It is easy to find that

(a) during the action of the external field (neglecting the anisotropy effects) the result of integration may be expressed as

$$\begin{aligned} \sin\theta(\tau+\tau_p) &= \frac{\tanh\eta + \sin\theta(\tau)}{1 + \tanh\eta\sin\theta(\tau)}, \\ \phi(\tau+\tau_p) &= \phi(\tau) - \eta, \end{aligned} \tag{5}$$

where $\eta = h_p\tau_p/(1+\alpha^2)$ and τ_p is the pulse length;

(b) when the external field is switched off the solution takes the form

$$\begin{aligned} \sin\chi(\tau+\tau_0) &= \frac{\lambda\sin\chi(\tau)}{(1-(1-\lambda^2)\sin^2\chi(\tau))^{1/2}}, \\ \psi(\tau+\tau_0) &= \psi(\tau) - \xi(\tau), \end{aligned} \tag{6}$$

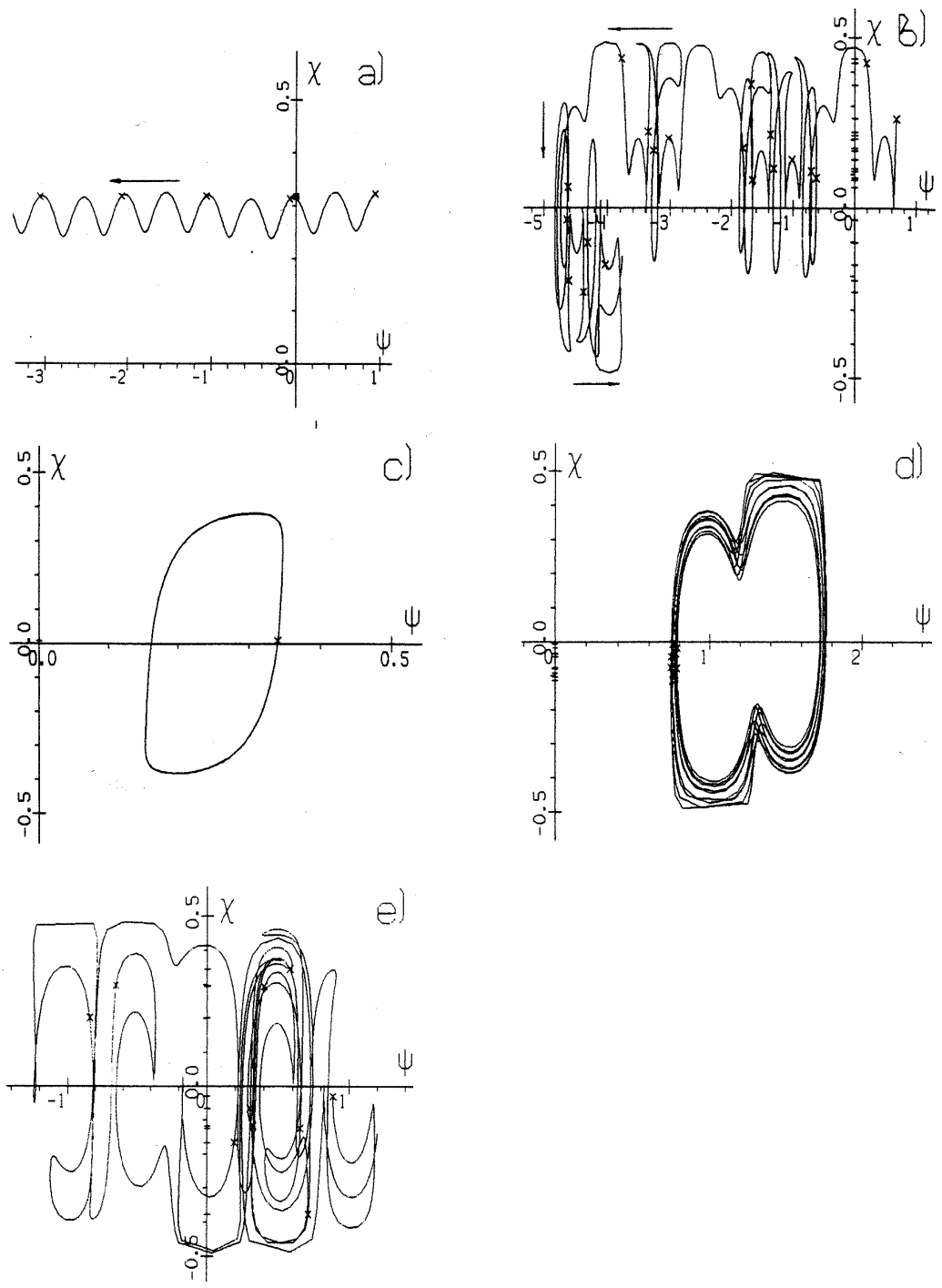

Figure 2: Fragments of phase trajectories for the case (i): $\chi(\tau)$ (in units of π) vs. $\psi(\tau)$ (in units of 2π) for the continuous time. Arrows show the direction of the time flow. Oblique crosses appear periodically and mark the time moments $\tau_N = N\tau_{\rm rf}, N = 1, 2, 3, \ldots$; their projections on the ordinate axis are marked by ticks. (a) A regular nutation with periodic oscillations for $h_{\rm rf} = 0.4$; (b) the transition to the motion in both upper and lower hemispheres for $h_{\rm rf} = 1.05$; regular (c) and chaotic (d) nutation around the axis orthogonal to the anisotrophy axis for $h_{\rm rf} = 1.4$ and 2.2, respectively; (e) complex chaotic motion on the sphere for $h_{\rm rf} = 2.4$.

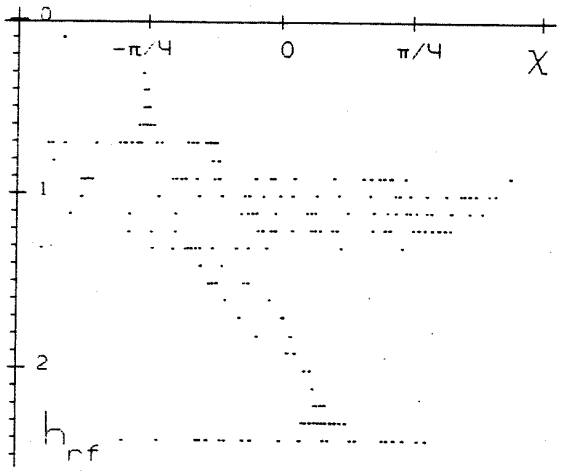

Figure 3: Bifurcation diagram for the case (i) for $h_0 = 0.2$.

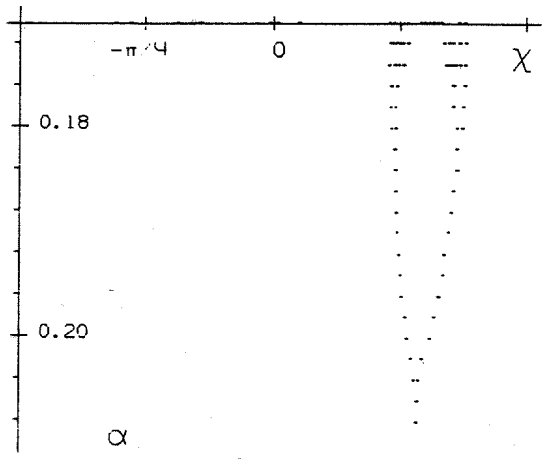

Figure 4: Period-doubling bifurcations in case (ii). The points on the horizontal show $\chi(\tau_N)$ for a fixed α value.

where $\xi(\tau) = \alpha^{-1} \ln\{[\lambda \sin\chi(\tau) + (1-(1-\lambda^2)\sin^2\chi(\tau))^{1/2}]/(1+\sin\chi(\tau))\}$, $\lambda = \exp(-\alpha\tau_0/(1+\alpha^2))$ and τ_0 is the interpulse gap.

Combining the expressions (5), (6) and using (4), we obtain the two-dimensional evolution map:

$$\begin{aligned} \theta_{N+1} &= F(\theta_N, \phi_N; \alpha, \lambda, \eta), \\ \phi_{N+1} &= G(\theta_N, \phi_N; \alpha, \lambda, \eta), \end{aligned} \tag{7}$$

where $\theta_N \equiv \theta(N(\tau_p + \tau_0)), \phi_N \equiv \phi(N(\tau_p + \tau_0))$. Now we can make the calculations using the formulae (7) instead of the numerical integration. Thus we obtain the system's "phase trajectory" in the discrete time scale (with temporal step $\tau_p + \tau_0$) by means of the step-by-step procedure.

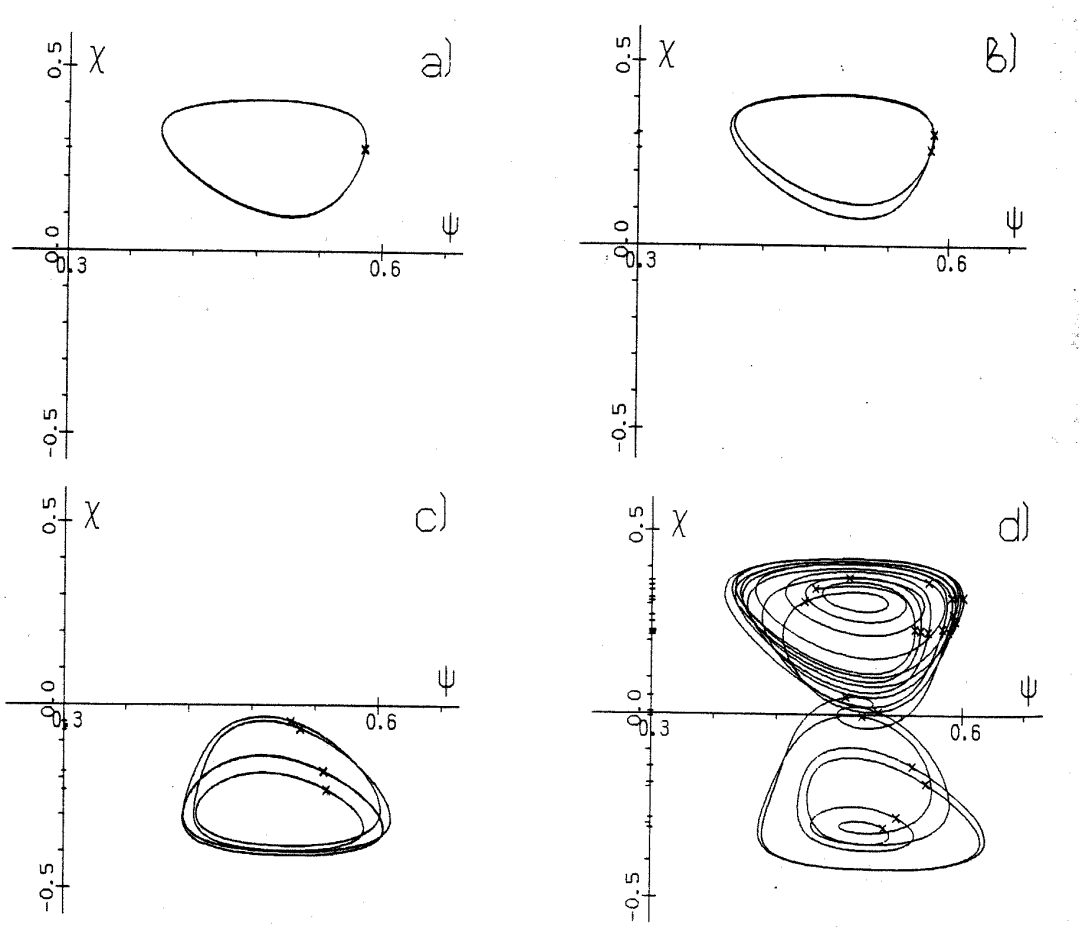

Figure 5: Fragments of the phase trajectories for the case (ii): $\chi(\tau)$ vs. $\psi(\tau)$ for the continuous time. A regular motion with periods: (a) $\tau_{\rm rf}$ for $\alpha = 0.206$; (b) $2\tau_{\rm rf}$ for $\alpha = 0.20$; (c) $4\tau_{\rm rf}$ for $\alpha = 0.176$; (d) a chaotic motion for $\alpha = 0.17$.

3 Numerical studies

In this section the dynamical behaviour of $\mathbf{m}$ is investigated by numerical solving the eqs. (2). Bifurcation diagrams (see figs. 1, 3 and 5) are constructed as plots of numerically obtained $\chi(\tau)$ (see formulae (4)) versus a bifurcation parameter. The points on the horizontal lines represent the values $\chi(\tau_N)$ for $\tau_N = N\tau_{\rm rf}, N = 1, 2, 3, \ldots$; here $\tau_{\rm rf} = 2\pi/\omega_{\rm rf}$ is the period of the external sinusoidal rf-field. In order to illustrate the pecularities of motion we use the plots of $\chi(\tau)$ vs. $\psi(\tau)$ for the continuous time.

We first consider bifurcation diagrams and phase trajectories for case (i). An example of the bifurcation diagram is shown in fig. 1. It is assumed that $\omega = 1, h_0 = 0, \alpha = 0.11$ and $h_{\rm rf}$ is the bifurcation parameter. This diagram indicates that there is a period $\tau_{\rm rf}$ motion for $h_{\rm rf} < 0.7$ and $1.3 < h_{\rm rf} < 2.1$; chaotic motion for $0.7 < h_{\rm rf} < 1.3$ and $h_{\rm rf} > 2.1$. The phase trajectory images (figs. 2a-e) help us to interpret this diagram. Notice that in the case under investigation the inversion $m_3 \to -m_3$ leaves eqs. (2) unchanged. If the rf-field amplitude is weak this leads to existence of two equivalent sorts of nutational motions: in the upper hemisphere ($0 < \chi < \pi/2$) and in the lower hemisphere ($-\pi/2 < \chi < 0$) (the respective rotations around the $\mathbf{e}_3$ axis have the opposite directions). Using numerical integration one can observe different types of motion.

Note that for simplification of the figures we draw the trajectory in a few rectangles defined by the expressions $-\pi/2 < \chi < \pi/2,\ 2\pi n < \psi < 2\pi(n+1),\ n = 0, \pm 1, \pm 2, \ldots$. Every rectangle corresponds to the whole sphere; after every rotation around the $\mathbf{e}_3$ axis the phase point passes from the initial rectangle to the neighbour one $(n \to n+1)$.

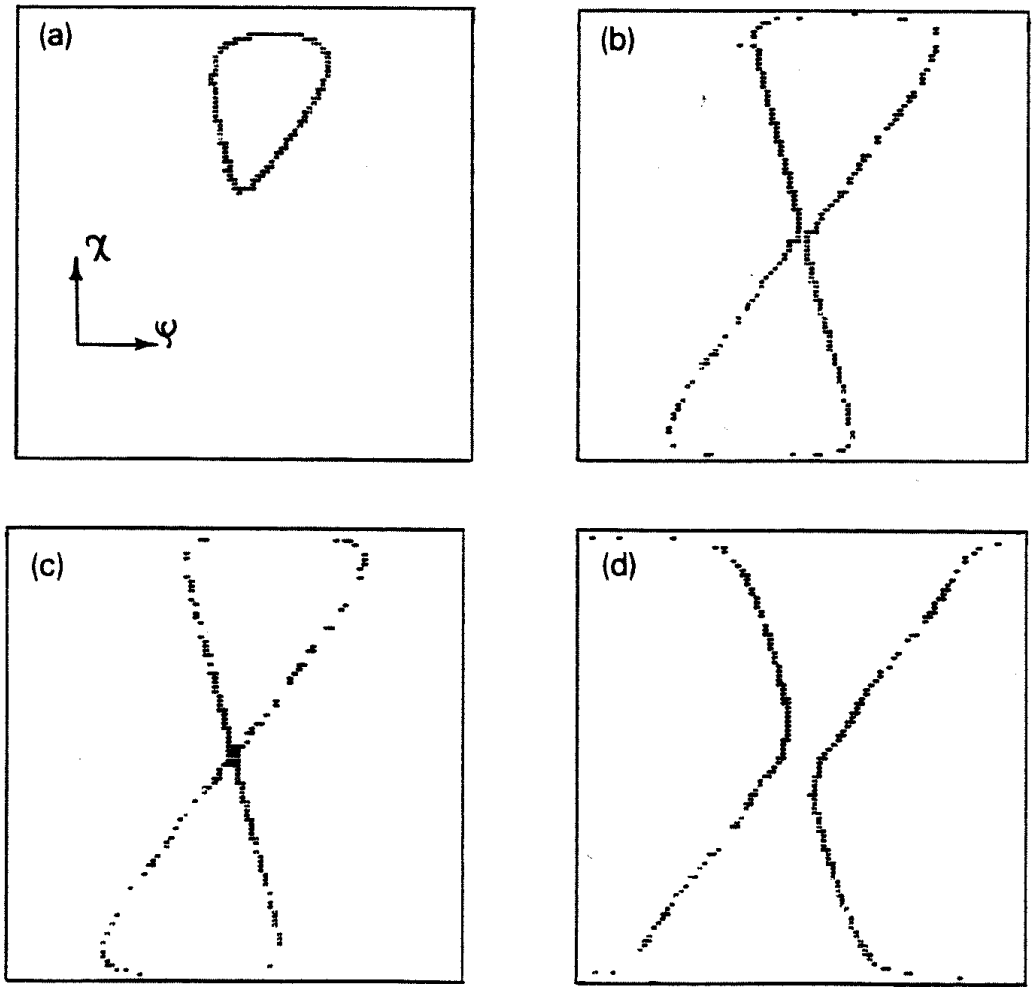

Figure 6: Phase portraits constructed by using the map iteration procedure.

As a first example, a regular nutation with periodicallv oscillating $\chi(\tau)$ for a weak incident field is shown in fig. 2a (the situation that the trajectory is located in the upper or lower hemispliere depends on the initial conditions). The increase of the rf-field intensity causes abrupt complication of the phase trajectories. The phase point often crosses an equator and moves chaotically in both the upper and lower hemispheres; this is shown in fig. 2b (note that a qualitatively similar behaviour have been discovered for the first time in the well-known Lorenz model [13]). A further increase of the rf-field amplitude causes the regular (fig. 2c) and chaotic (fig. 2d) nutations around the $\mathbf{e}_2$ axis, and then the combined chaotic nutation around $\mathbf{e}_2$ and $\mathbf{e}_3$ axes (fig. 2e). One of the bifurcation diagrams for the case (i) for $h_0 \neq 0$ is shown in fig. 3; it contains the pattern similar to that of in fig. 1.

The bifurcation diagram in the case (ii) with $h_0 = 0.6, h_{\mathrm{rf}} = 0.2, \omega = 0.7$ is shown in fig. 4; here α is the bifurcation parameter. In this case we have seen the route to chaos through the

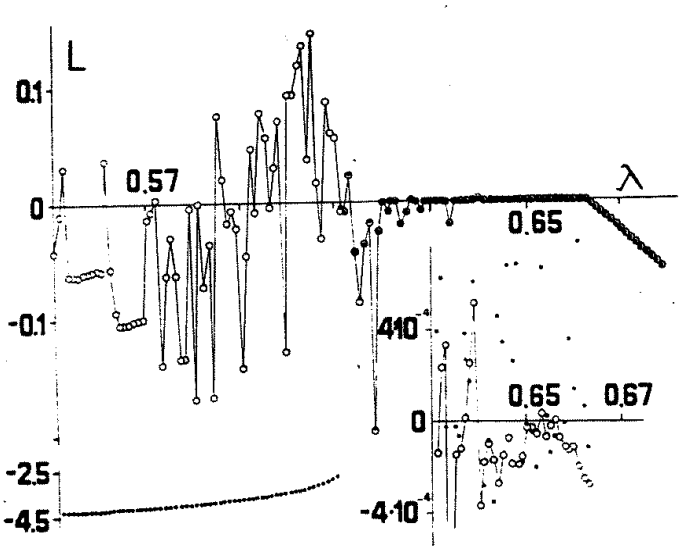

Figure 7: The maximal Lyapunov exponent for the case (iii). There is the 10-cycle for $0.552 < A < 0.56$ and the 12-cycle for $0.564 < A < 0.569$. The inlay contains an enlarged fragment of the plot.

sequence of the period-doubling bifurcations; the first three bifurcations can be identified in fig. 4. The examples of the phase portraits of various regimes from periodic with period $\tau_{\rm rf}$ to chaotic via period-doubling are shown in figs. 5a-d. Note that fig. 5d resembles the well-known Lorentz attractor.

In the last case (iii) we have constructed the system's phase portraits (fig. 6) consisting of the isolated phase points $(\chi(\tau_N),\ \psi(\tau_N))$, $\tau_N = N\tau_{\rm rf}$. Calculations have been carried out by applying formulae (7) for $\alpha = 0.3, \eta = 0.785$, λ is variable. In this case it is easy to observe various attractor transformations including merging of the attractor components. Namely, for $\lambda = 0.627$ (the chaotic motion) there are two symmetrically located attractor components; each of them has the form of a loop and is trapped in its own basin of attraction (in fig. 6a only one of these components is shown). With λ decreasing the attractor components merge and this leads to the formation of a new two-component attractor. This attractor consists of a chaotic component (shown in figs. 6b-d) and a stable point.

It is convenient to combine the phase portraits analysis with the calculation of the maximal Lyapunov exponent (MLE) [1]. We have to remind that if the MLE is negative then the nearby trajectories converge onto the attractor and the motion is regular; the positive MLE corresponds to the chaotic motion. From fig. 7 one can see the alternation of the regular and chaotic motion zones as λ changes. Graphs corresponding to the different components of the attractor are marked by points and rings respectively.

4 Concluding remarks

We showed that it is possible to observe complex regimes of motion even for a simplest model describing the spatial homogeneous magnetization dynamics in ferromagnets. This system demonstrates some well-known dynamical features (such as cascades of the subharmonic bifurcations and existence of the multicomponent attractors) typical for nonlinear systems. Thus, the magnetization dynamics under the external field action would be interesting to study more

comprehensively.

References

[1] A.J. Lichtenberg and M.A. Lieberman, *Regular and Stochastic Motion* (Springer-Verlag, New York, 1983).

[2] H.G. Schuster, *Deterministic Chaos* (Physik-Verlag Weinheim, 1984).

[3] F.C. Moon, *Chaotic Vibrations* (John Wiley, New York 1987).

[4] F.H. de Leeuw, R. van der Doel and U. Enz, Rep.Prog.Phys. **43** (1980) 689.

[5] G.M. Rodichkov, N.P. Lyakhovskij, P.D. Kim and V. Presnetsov, Izvestija Vuzov (Fizika) N**7** (1969) 140 (in Russian).

[6] C.D. Olson and A.V. Pohm, J.Appl.Phys. **29** (1958) 27.

[7] P.R. Gillette and K. Oshima, J.Appl.Phys. **29** (1958) 1465.

[8] W. Dietrich and W. Proebster, Electronische Rundsch. **14** (1960) 47.

[9] D.O. Smith, Phys.Rev. **104** (1956) 1280.

[10] G. Vogler, Phys.Stat.Sol. **2** (1962) 1241.

[11] U. Rosler, Phys.Stat.Sol. **3** (1963) 3.

[12] T.L. Gilbert, Phys.Rev. **100** (1955) 1243.

[13] E.N. Lorentz, J.Atmos.Sci. **20** (1963) 130.